

Studying the internal structure of exotic hadrons and bound states using spectroscopy and complementary techniques with ALICE

Sonali Padhan (for the ALICE Collaboration)^{a,*}

^a*Department of Physics, Indian Institute of Technology Bombay
Powai, Mumbai, 400076, India*

E-mail: sonali.padhan@cern.ch

The internal structure of hadrons, bound states, and the existence of excited states can be studied using hadron spectroscopy. Complementary information can be obtained using the multi-particle correlation technique, from which it is possible to infer the existence and properties of bound states, and by measuring the hadron yields and comparing them with predictions of the statistical hadronization model. The latter has proved to be a powerful tool to calculate hadron abundances and allows us to deduce indirectly the number of excited states of a given hadron species, including weakly bound states such as hypernuclei.

These proceedings describe recent results on short-lived exotic resonance production, hypernuclei structure, and searches for exotic bound states in different collision systems. The implications of these results on the hadron structure and possible excited states are also discussed.

*16th International Conference on Heavy Quarks and Leptons (HQL2023)
28 November-2 December 2023
TIFR, Mumbai, Maharashtra, India*

*Speaker

1. Introduction

In high-energy physics, the study of hadronic matter, particularly the study of resonance production, excited states of hadrons, and the investigation of hypernuclei, plays a crucial role in unravelling the fundamental properties of the strong force. Besides these studies, advanced spectroscopy techniques offer a nuanced comprehension of the internal structure of hadron. The study of hadronic resonances is crucial for understanding the hadronic phase in high-energy heavy-ion collisions. Since the lifetimes of exotic resonances are comparable to the duration of the hadronic phase, these resonances act as sensitive probes for exploring phenomena like rescattering and regeneration. These processes can influence resonance yields and contribute to shaping transverse momentum spectra.

The classification of standard hadrons has traditionally relied on the quark model. Although this model effectively describes many established states, certain hadrons exist, including observed resonances, displaying properties indicative of an exotic structure with unconventional configurations. In particular, understanding the quark composition of light scalar mesons the traditional understanding of their quark content remains a topic of continuous investigation. Numerous theoretical interpretations are explored to determine if particles' internal structure follows compact multi-quark states or tends more towards a molecular-like arrangement.

In statistical hadronisation models (SHM) light nuclei are believed to be originated from a source in local thermodynamic equilibrium describing overall yields in nucleus–nucleus collisions but lacking detailed information like momentum distributions [1, 2]. Conversely, The coalescence model generally explains how nuclei are formed from nucleons released by a hot fireball as it cools and expands. The basic version of these models assumes the creation of a bound state if nucleons are sufficiently close in momentum space, overlooking spatial correlations between nucleons. However, recent advanced implementations consider the overlap between nucleon phase space and the Wigner density function of the final bound state, providing a more detailed calculation of the coalescence probability [3, 4]. Studying the lifetimes and binding energies of hypernuclei offers insights into the interaction between hyperons and nucleons.

2. Experimental and analysis details

The ALICE detector at the Large Hadron Collider (LHC) is specifically designed for probing the quark–gluon plasma through heavy-ion collisions. Its sub detectors used for the analyses are the Inner Tracking System (ITS), the Time Projection Chamber (TPC), The Time-Of-Flight (TOF), and the V0A and V0C detectors. The ITS is used for tracking charged particles and determining the primary vertex of collisions. The TPC is used to track the charged particles as they traverse through a gas volume and provides particle identification via energy loss. The TOF detector measures the time taken by charged particles to travel from the collision point to the detector. When combined with the particle's momentum, this information enables accurate particle identification. The V0A and V0C detectors are arrays of scintillator detectors used for triggering and event characterization in heavy-ion collisions and cover the pseudorapidity intervals $2.8 < \eta < 5.1$ and $-3.7 < \eta < -1.7$, respectively. They contribute to event triggering and selection based on the event multiplicity. The Zero Degree Calorimeter (ZDC) is used to obtain the multiplicity percentile distribution.

Specifically, the ZNA definition is used focusing on the Pb-going side. This classification aids in studying collision centrality and provides insights into the initial conditions and properties of the Quark-Gluon Plasma in heavy-ion collisions. [5].

3. Resonances production

The properties of the hadron gas phase, formed post hadronization, can be investigated through the measurement of short-lived resonance yields. Given the comparable lifetimes of these resonances to the hadron gas phase, their yields are affected by rescattering effects involving decay daughters interacting with other hadrons. Furthermore, regeneration effects, reflecting the back reaction to their decay, contribute to the overall impact on resonance yields. The ALICE Collaboration has measured the yield ratios of resonances with varying lifetimes compared to stable hadrons.

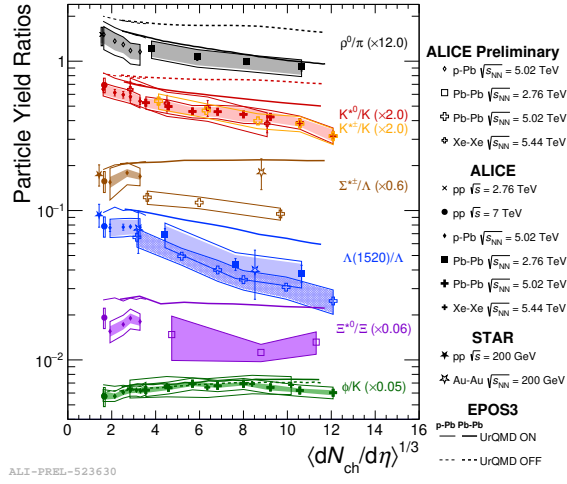


Figure 1: Particle yield ratios ρ^0/π , K^{*0}/K , $K^{*\pm}/K$, $\Sigma^{*\pm}/\Lambda$, $\Lambda(1520)/\Lambda$, Ξ^{*0}/Ξ , ϕ/K as a function of multiplicity for pp, p–Pb, Xe–Xe, and Pb–Pb collisions, with comparisons to EPOS3 predictions and STAR data.

Figure 1 shows the ratio of resonance yields to those of long-lived particles as a function of $(dN_{ch}/d\eta)^{1/3}$ for various resonances in several collision systems and energies, measured by the ALICE and STAR [6] Collaborations.

The ratios of ρ^0/π , K^{*0}/K , $K^{*\pm}/K$, and $\Lambda(1520)/\Lambda$ exhibit a decreasing trend from peripheral to central collisions. In contrast, the ratios of $\Sigma^{*\pm}/\Lambda$, Ξ^{*0}/Ξ , and ϕ/K remain relatively constant across all systems and centrality classes. The recent measurement of $K^{*\pm}$ aligns with previous findings for K^{*0} in Pb–Pb collisions at $\sqrt{s_{NN}} = 5.02$ TeV. These results suggest the prevalence of rescattering effects over regeneration in the hadronic phase. Notably, $\Lambda(1520)/\Lambda$ experiences more suppression than K^{*0}/K and $K^{*\pm}/K$ despite its longer lifetime, emphasizing the intricate interplay of resonance characteristics with multiplicity. A comparison with the EPOS3 with UrQMD [7] model indicates general agreement with the experimental measurements. It's important to note that predicting resonance suppression solely based on lifetime is inadequate; factors like the mean

free path within the hadron gas phase and achieving (partial) chemical equilibrium are crucial for a comprehensive understanding of resonance behaviour in such environments.

4. Structure of Exotic hadrons

The $f_0(980)$ and γ_s yield ratios in pp collisions at $\sqrt{s} = 5.02$ TeV have been compared to γ_s -CSM (Canonical statistical model) predictions in two scenarios [8]. It incorporates the incomplete equilibration of strangeness by introducing a strangeness saturation factor $\gamma_s \leq 1$. In the first scenario when $f_0(980)$ has total strangeness ($|S| = 0$), the model predicts higher yield ratios at low multiplicities ($\langle dN_{ch}/d\eta \rangle$) compared to the second assumption of $|S| = 2$. Remarkably, these predictions converge and closely match when the multiplicity surpasses the average charged-particle multiplicity ($\langle dN_{ch}/d\eta \rangle$) of about 100 [9].

In p–Pb collisions at $\sqrt{s_{NN}} = 5.02$ TeV, $f_0(980)$ to K^{*0} yields ratio in multiplicity intervals relative to low-multiplicity is shown in the left side of Figure 2. The γ_s -CSM model prediction for $f_0(980)$ under both $|S| = 0$ and $|S| = 2$ strangeness content assumptions exhibit distinct trends. The observed decreasing trend in the double ratio with increasing multiplicity aligns with the assumption of zero hidden strangeness for $f_0(980)$. Consequently, the decreasing trend in the double ratio of $f_0(980)$ to K^{*0} suggests no effective strangeness enhancement for $f_0(980)$. There is a noticeable increasing trend for the $f_0(980)/K^{*0}$ yield ratio in the CSM prediction with two hidden strange quarks indicating a mild increase in multiplicity, contrary to the experimental result. Notably, the measured trend qualitatively agrees with the $|S| = 0$ scenario where $f_0(980)$ lacks strangeness.

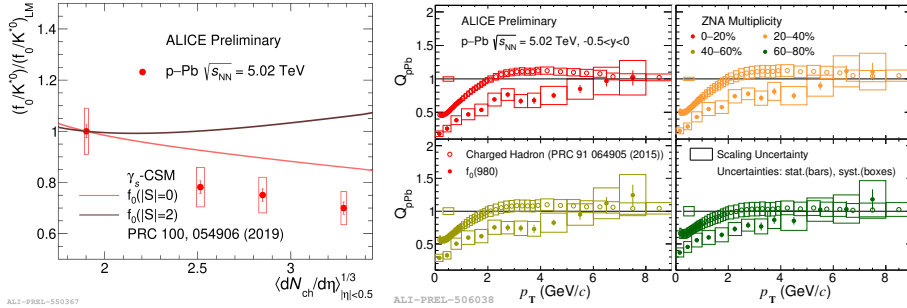


Figure 2: (Left side) Double ratio of $(f_0(980)/K^{*0})/(f_0(980)/K^{*0})_{LM}$ (where low multiplicity class (LM) is 60–100%) compared with γ_s -CSM model predictions for $(|S| = 0)$ and $(|S| = 2)$ in p–Pb collisions at $\sqrt{s_{NN}} = 5.02$ TeV as a function of charged-particle multiplicity raised to the power of 1/3. (Right side) Nuclear modification factor for $f_0(980)$ yield for different ZNA multiplicity classes.

Recent estimations of the nuclear modification factor for $f_0(980)$ in p–Pb collisions are shown on the right side of Figure 2. The results demonstrate a suppression in $f_0(980)$ yield at low p_T , surpassing that of charged hadrons, particularly in more central collisions. This suppression suggests potential rescattering effects. Importantly, there is no observed Cronin peak in the intermediate p_T region. Given that baryons typically exhibit a more pronounced Cronin peak compared to conventional mesons [10], the absence of a significant Cronin-like enhancement for $f_0(980)$ may suggest its composition as a conventional meson structure consisting of two quarks.

5. Hypertriton Investigation

Hypernuclei, bound states formed by nucleons and hyperons like the Λ baryon, offer unique insights for hyperon–baryon and hyperon–hyperon interactions. Due to their weakly bound nature, hypernuclei serve as valuable probes, to differentiate between different production scenarios for light nuclei.

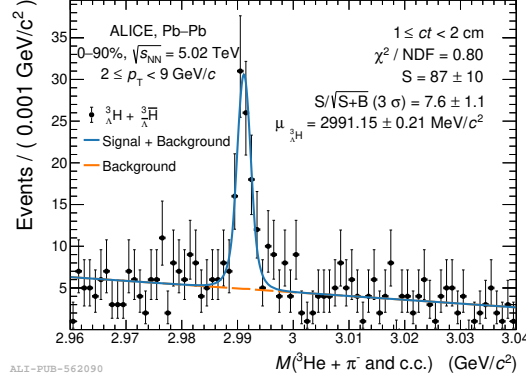


Figure 3: Invariant mass distribution of hypertriton from the mesonic decay channel ${}^3_{\Lambda}\text{H} \rightarrow {}^3\text{He} + \pi^-$ (B.R. $\approx 25\%$)

In Pb–Pb collisions at the LHC, approximately the same number of ${}^3_{\Lambda}\text{H}$ and ${}^3_{\Lambda}\bar{\text{H}}$ will be produced. The ${}^3_{\Lambda}\text{H}$ is reconstructed through the charged two-body channel ${}^3_{\Lambda}\text{H} \rightarrow {}^3\text{He} + \pi^-$ (and the corresponding charge-conjugated particles for ${}^3_{\Lambda}\bar{\text{H}}$). The identified ${}^3\text{He}$ and π tracks are then used to reconstruct the ${}^3_{\Lambda}\text{H}$. The invariant mass distribution of the ${}^3_{\Lambda}\text{H}$ is shown in Figure 3.

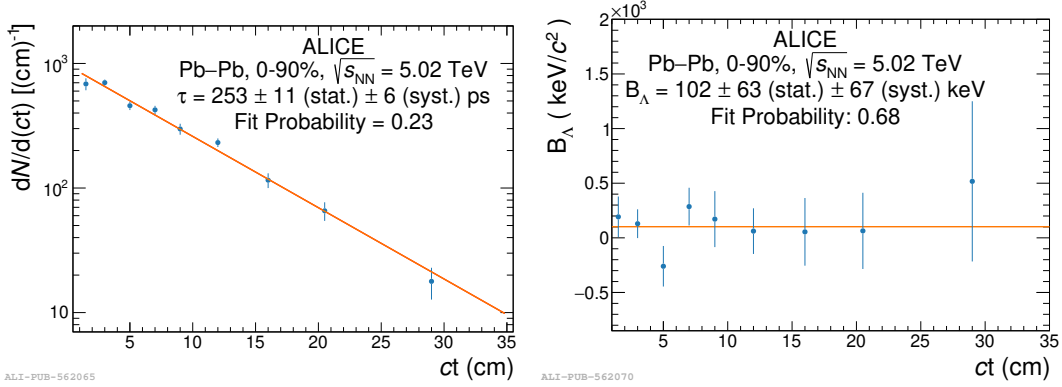


Figure 4: (Left side) Exponential decay spectrum as a function of the proper decay length for ${}^3_{\Lambda}\text{H}$. (Right side) B_{Λ} measurement as a function of the proper decay length.

The lifetime of ${}^3_{\Lambda}\text{H}$ is extracted by analyzing the proper decay length spectrum shown on the left side of Figure 4. The spectrum is modelled as an exponential decay as a function of the proper decay length for ${}^3_{\Lambda}\text{H}$. The blue points represent the measured yield, while the orange line represents the best fit for the measurement.

The separation energy (B_{Λ}) of ${}^3_{\Lambda}\text{H}$ as shown in the right side of Figure 4 is determined within each ct interval using the ${}^3_{\Lambda}\text{H}$ mass ($\mu_{{}^3_{\Lambda}\text{H}}$) obtained from the fit, the deuteron mass is taken

from CODATA [11] and the Λ mass obtained from the PDG [12]. The reconstructed value of $\mu_{\Lambda^3\text{H}}$ is influenced by the imperfect correction for the energy loss of the daughter particles. The measurements for the ${}^3_{\Lambda}\text{H}$ lifetimes, as well as B_{Λ} obtained are $\tau = (253 \pm 11 \text{ stat} \pm 6 \text{ syst}) \text{ ps}$; and $B_{\Lambda} = (102 \pm 63 \text{ stat} \pm 67 \text{ syst}) \text{ keV}$ respectively.

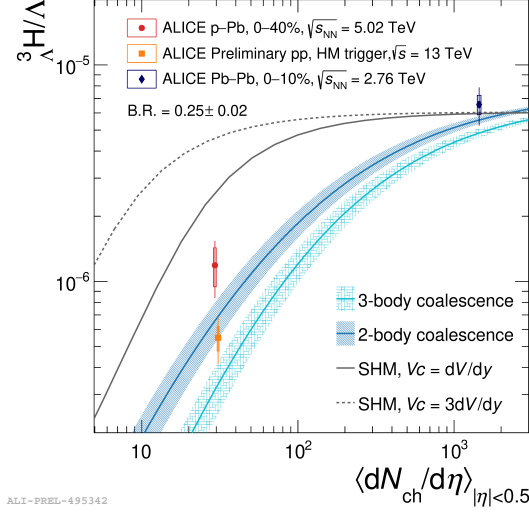


Figure 5: Hypertriton over Λ ratio as a function of the mean charged-particle multiplicity density in pp high multiplicity, p–Pb collisions and Pb–Pb collisions are compared to the predictions from SHM.

In small collision systems, hypertriton production has been studied through experiments in two scenarios: pp collisions at 13 TeV and p–Pb collisions at 5.02 TeV. Notably, a substantial separation exists between the predictions derived from the SHM and the coalescence model.

In the case of p–Pb collisions, the ${}^3_{\Lambda}\text{H}/\Lambda$ ratio as shown in Figure 5 is well described by the two-body coalescence prediction. However, the three-body coalescence formulation is somewhat disfavored by the observed data. In contrast, in the central Pb–Pb collisions, the experimental data exhibit consistency with predictions from both coalescence and the Statistical Hadronization Model. This suggests that the production mechanism for hypertritons in central Pb–Pb collisions can be reasonably explained by either coalescence or statistical hadronization processes. The observed discrepancy between predictions from different models, particularly in small-collision systems, highlights the importance of further investigations into hypertriton production mechanisms. These findings contribute to our understanding of the complex dynamics involved in different collision scenarios and provide valuable insights into the properties of the produced hypernuclei.

References

- [1] A. Andronic, P. Braun-Munzinger, K. Redlich, and J. Stachel, “Decoding the phase structure of QCD via particle production at high energy”, *Nature* **561** (2018) 321–330, [arXiv:1710.09425](https://arxiv.org/abs/1710.09425) [nucl-th].
- [2] ALICE Collaboration, S. Acharya *et al.*, “Production of ${}^4\text{He}$ and ${}^4\overline{\text{He}}$ in Pb–Pb collisions at $\sqrt{s_{\text{NN}}} = 2.76 \text{ TeV}$ at the LHC”, *Nucl. Phys. A* **971** (2018) 1–20, [arXiv:1710.07531](https://arxiv.org/abs/1710.07531) [nucl-ex].

- [3] M. Mahlein, L. Barioglio, F. Bellini, L. Fabbietti, C. Pinto, B. Singh, and S. Tripathy, “A realistic coalescence model for deuteron production”, *Eur. Phys. J. C* **83** (2023) 804, [arXiv:2302.12696 \[hep-ex\]](#).
- [4] **ALICE** Collaboration, J. Adam *et al.*, “Production of light nuclei and anti-nuclei in pp and Pb-Pb collisions at energies available at the CERN Large Hadron Collider”, *Phys. Rev. C* **93** (2016) 024917, [arXiv:1506.08951 \[nucl-ex\]](#).
- [5] **ALICE** Collaboration, K. Aamodt *et al.*, “The ALICE experiment at the CERN LHC”, *JINST* **3** (2008) S08002.
- [6] **STAR** Collaboration, M. M. Aggarwal *et al.*, “ K^{*0} production in Cu+Cu and Au+Au collisions at $\sqrt{s_{NN}} = 62.4$ GeV and 200 GeV”, *Phys. Rev. C* **84** (2011) 034909, [arXiv:1006.1961 \[nucl-ex\]](#).
- [7] K. Werner, T. Hirano, I. Karpenko, T. Pierog, S. Porteboeuf, M. Bleicher, and S. Haussler, “Gribov-Regge theory, partons, remnants, strings - and the EPOS model for hadronic interactions”, *Nucl. Phys. B Proc. Suppl.* **196** (2009) 36–43.
- [8] V. Vovchenko, B. Dönigus, and H. Stoecker, “Canonical statistical model analysis of p-p, p-Pb, and Pb-Pb collisions at energies available at the CERN Large Hadron Collider”, *Phys. Rev. C* **100** (2019) 054906, [arXiv:1906.03145 \[hep-ph\]](#).
- [9] **ALICE** Collaboration, S. Acharya *et al.*, “ $f_0(980)$ production in inelastic pp collisions at $\sqrt{s} = 5.02$ TeV”, *Phys. Lett. B* **846** (2023) 137644, [arXiv:2206.06216 \[nucl-ex\]](#).
- [10] **ALICE** Collaboration, J. Adam *et al.*, “Multiplicity dependence of charged pion, kaon, and (anti)proton production at large transverse momentum in p-Pb collisions at $\sqrt{s_{NN}} = 5.02$ TeV”, *Phys. Lett. B* **760** (2016) 720–735, [arXiv:1601.03658 \[nucl-ex\]](#).
- [11] P. J. Mohr, D. B. Newell, and B. N. Taylor, “CODATA Recommended Values of the Fundamental Physical Constants: 2014”, *Rev. Mod. Phys.* **88** (2016) 035009, [arXiv:1507.07956 \[physics.atom-ph\]](#).
- [12] **Particle Data Group** Collaboration, P. A. Zyla *et al.*, “Review of Particle Physics”, *PTEP* **2020** (2020) 083C01.